



# Performance evaluation of three optical particle counters with an efficient “multimodal” calibration method

Michael Heim<sup>a</sup>, Benjamin J. Mullins<sup>b,\*</sup>, Heinz Umhauer<sup>a</sup>, Gerhard Kasper<sup>a</sup>

<sup>a</sup>Institut für Mechanische Verfahrenstechnik und Mechanik, Gas-Partikel-Systeme, Universität Karlsruhe (TH), D-76128 Karlsruhe, Germany

<sup>b</sup>Centre of Excellence in Cleaner Production, Curtin University of Technology, GPO Box U1987, Perth WA 6845, Australia

Received 30 January 2008; received in revised form 16 June 2008; accepted 22 July 2008

## Abstract

The sizing accuracies of two widely used yet hitherto unevaluated optical particle counters (OPCs—Grimm Model 1.109 and Palas Model WELAS 2100) as well as one high-resolution, non-commercial OPC were evaluated. The measured data were compared to scattering intensity calculations based on Mie theory. Additionally, the counting efficiency for all three counters was measured, as was the influence of coincidence effects for the OPC with the lowest (manufacturer specified) upper concentration limit.

Beside the traditional polystyrene latex calibration, a little-known, very fast and precise “multimodal” calibration method was used, which is based on the simultaneous generation of up to eight sharp multiple-charge modes from polydisperse di-ethyl-hexyl-sebacate (DEHS) particles by electrical mobility classification.

© 2008 Elsevier Ltd. All rights reserved.

**Keywords:** Optical particle counter (OPC); Calibration; Counting efficiency; Coincidence; Differential mobility analyser (DMA); Condensation particle counter (CPC)

## 1. Introduction

Optical particle counters (OPCs) are routinely used for real-time aerosol characterization in the particle size range of approximately 0.3–20 µm. They are applied to everything from low concentration measurements such as clean room or PM<sub>x</sub> monitoring in ambient air, to highly concentrated industrial aerosols, e.g. for industrial filter testing under realistic conditions.

For the latter application, OPCs are often the only suitable type of (on-line) device capable of operating at high concentrations up to  $1 \times 10^7$  p/cm<sup>3</sup> ([Sachweh, Umhauer, Ebert, Buttner, & Friehmelt, 1998](#)). Since their sizing accuracy depends strongly on the refractive index of the particle material, frequent calibration and recalibration of such devices is a necessity. Most commonly, the manufacturer-supplied calibration curve (between light scattering, signal intensity and particle size) is based on monodisperse polystyrene latex (PSL) aerosols, which have a refractive index  $m = 1.59$ . However, during normal use OPCs are often required to measure particles of very different refractive indices (and shape factors), which understandably affects their calibration. Among such aerosol particles, oil mists are important industrially; they are a standard for filter testing; and oil droplet aerosols are very common in scientific research as

\* Corresponding author. Tel.: +61 8 9266 2267; fax: +61 8 9266 4811.

E-mail address: [b.mullins@curtin.edu.au](mailto:b.mullins@curtin.edu.au) (B.J. Mullins).

well, as they are easy to generate and usually spherical in shape. The accurate measurement of such droplets in terms of size and concentration is therefore important. Oils are generally lower in (real) refractive index than PSL, which results in a reduction of scattered light intensity. In addition, the imaginary component of their refractive index (Card & Jones, 1991) is often higher (Nagy, Szymanski, Gal, Golczewski, & Czitrowsky, 2007), usually resulting in a further reduction due to absorption. For very fine aerosols, this may, in some cases, also affect the lower detection limit and hence the counting efficiency of the OPC.

Among the widely used types of commercial OPC are the Model 1.109 (Grimm Aerosol Technik), a compact laser-based device with wide light collection angle designed for environmental and industrial monitoring, and the WELAS 2100 (Pallas), which uses a 90° scattering angle in combination with a high-intensity white light source. Because of its excellent resolution and wide operating range (Umhauer, Berbner, & Hemmer, 2000), this latter type of design is also a popular laboratory instrument and exists in various optical configurations, all based on white light and a 90° scattering angle. The use of white light minimises or eliminates the well-known oscillation in the calibration curve often observed in the Mie range (Raasch & Umhauer, 1977). Each of these devices requires calibration curves for the various test aerosols, or at least an estimate for the deviations in size from the manufacturer's PSL calibration, which are rarely available in the literature. Although OPC calibration should be a matter of routine, efficient calibration procedures with specific particle materials are often cumbersome to set up, because a broad range of monodisperse size classes in the super-micron size range must be generated.

In this paper, we describe an efficient “multimodal” calibration procedure to generate particles in the size range of about 0.1–5 µm, and we then apply this procedure to the above mentioned three types of OPCs. The calibration technique has been mentioned at least once before in the literature (Chen, Cheng, & Yeh, 1986) but may have gone unnoticed at that time. It is performed using broadly distributed oil aerosol, which is classified by a differential mobility analyser (DMA) to produce a series of multiple charge peaks well into the super-micron size range. This feature permits the generation of up to eight particle sizes in one pass. The calibration aerosol used here was di-ethyl-hexyl-sebacate (DEHS)—an oil often used in laboratory studies due to its low vapour pressure; DEHS possesses similar properties to many other oils utilised industrially. In addition, the counters were calibrated with PSL, in order to determine the effect of refractive index and the counting efficiency at the lower size limit.

### *1.1. OPCs examined in this work*

#### *1.1.1. UKA A10*

**Fig. 1A** shows a schematic of the UKA A10, which was designed and manufactured at the Universität Karlsruhe. Since its design is the basis for a number of other devices in wide use, its calibration is of some interest. The A10 (as well as the WELAS OPC discussed next) uses an intense source of white light (Osram XBO-75 Xenon short arc lamp) to illuminate a nearly cubic particle sensing volume of  $6.55 \times 10^4 \mu\text{m}^3$  located at the centre of the aerosol flow path. This volume is defined by a combination of apertures placed in the optical path of the illumination and the two sensing (photomultiplier) branches, which are arranged at an observation angle of 90° opposing each other. Although the A10 could also function with a single detector arm, the “twin-arm” design (Sachweh et al., 1998) with two photomultiplier paths is advantageous in identifying and suppressing erroneous light signals emitted by partially illuminated particles crossing the sensing volume (at or near the edges).

Due to its optical arrangement, the A10 (as well as the WELAS device discussed next) detects, sizes and counts particles in a very precisely defined sensing volume which is much smaller than the flow path. This is advantageous, especially at high particle concentrations. However, concentration measurements require an independent calibration because they are actually based on the particle flux through that sensing volume.

#### *1.1.2. Palas WELAS 2100*

**Fig. 1B** shows an approximate schematic of the WELAS 2100 (Palas, Karlsruhe). The basic optical configuration is similar to the A10, with a white light source and a 90° scattering angle. A peculiarity of the Model 2100 is the special shape of its optical sensing volume (see the inset in **Fig. 1B**) which has a T-shaped cross-section, permitting the use of only one PMT (Mölter & Keßler, 2004a) instead of two as in the A10. This patented T-shape (Mölter & Munzinger, 1998; Mölter & Keßler, 2004b) allows the elimination of false signals from particles travelling through the border zone on the basis of pulse length. It should be noted that the WELAS devices are generally designed for portability; thus the sensing volume of the Model 2100 is connected to the remainder of the device via optical fibre.

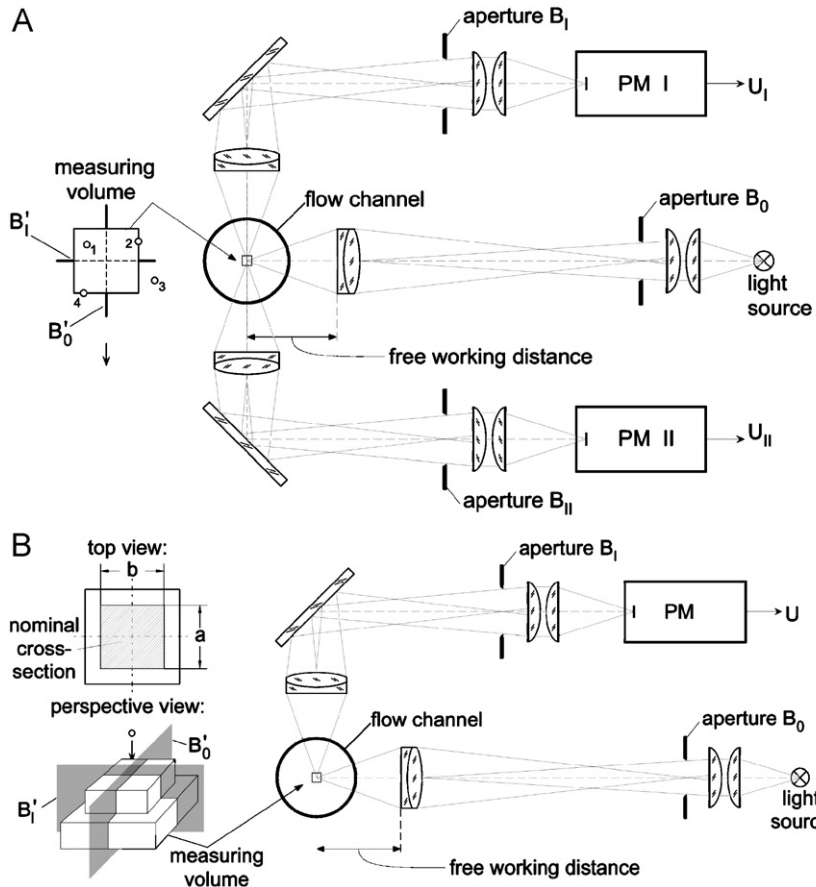


Fig. 1. Schematic designs of the A10 (top) and the WELAS (bottom), representing the twin-arm OPC with cubic measuring volume (after Dittler, 2001); and the single-arm OPC with T-shaped measuring volume (Umhauer, Meyer, & Schiel, 2008), respectively.

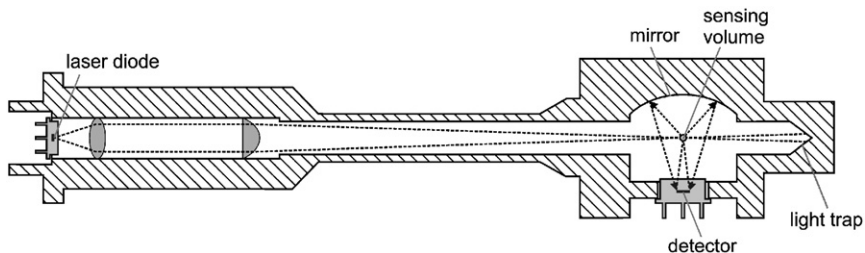


Fig. 2. Schematic of the cross-section of the Grimm 1.109 OPC. The aerosol flow through the sensing volume is perpendicular to the image plane.

Two calibration curves were available with the device tested—a curve for PSL particles (refractive index  $m = 1.59$ ), and the second curve for oil particles ( $m = 1.45$ ).

### 1.1.3. Grimm 1.109

This OPC (Fig. 2) uses a 683 nm laser diode to illuminate the aerosol beam, and a wide-angle collector optic to detect light pulses with a photo diode. The optical arrangement (mean scattering angle 90°) collects the scattered light with a parabolic mirror (120°) on one side and an additional 18° on the opposing side. The wide angle optic increases the total amount of scattered light detected by the photo sensor, close to the Rayleigh scattering domain. This improves

the signal to noise ratio, which leads to a decrease in the minimum particle size which can be detected (which is specified by the manufacturer as  $0.25\text{ }\mu\text{m}$ ). The optic design also smoothes out Mie scattering undulations caused by the monochromatic illumination; the sensitivity to particle shape is also reduced.

As opposed to the two other OPCs, the 1.109 counts all particles entering the chamber; it thus measures absolute particle concentrations and should be more accurate in this regard. However, this design also increases the coincidence error and reduces the upper concentration limit. This is not a problem because the device is primarily intended to measure environmental aerosols (which are usually at a lower concentration), whereas the other two are principally used for the measurement of industrial aerosols (e.g. filter testing).

## 2. Calculation of theoretical response curves

The theoretical signal response curves of two of the three OPCs were calculated by a computer program developed by [Vetter \(2004\)](#), based on the well-known Mie algorithm developed by [Bohren and Huffman \(1998\)](#). This calculation requires certain information concerning the OPC, namely the optical configuration (detection angle and detector distance), the properties of the detector (size of the detection array and photometric sensitivity), as well as the specifications of the light source (wavelength distribution and intensity distribution in the sensing volume). Where such data were available (A10 and Grimm 1.109), the theoretical responses were calculated and compared with the experimentally determined responses, as will be shown later.

For the A10, the wavelength distribution of the light source (XBO-75 lamp; data supplied by the lamp manufacturer) and the spectral sensitivity of the Bi-alkali photomultiplier had to be convoluted ([Fig. 3](#)) and the resulting distribution discretized between 275 and 685 nm into 82 wavelength channels. The light scattering response of the A10 was then calculated by superposition of the angular intensity distributions for each wavelength interval. Some fluctuations remain evident in the derived signal, which could have been smoothed out by further increasing the degree of discretization to 410 channels. Since this would have increased the computation times substantially, all theoretical response curves of the A10 are based on a discretization of 82 channels.

The WELAS curves could not be calculated because information about spectral sensitivity was unavailable, but may be considered similar to the A10. The Grimm OPC uses monochromatic light, which eliminates the need for such a procedure.

[Fig. 4](#) shows a comparison of the calculated OPC response curves. Clearly, the white light instrument A10 has the smoothest, monotonic curve, although at the expense of intensity below  $1\text{ }\mu\text{m}$  caused by the narrow collection angle of the instrument. The wide angle laser OPC 1.109 also has a relatively smooth curve due to the wide angle collection

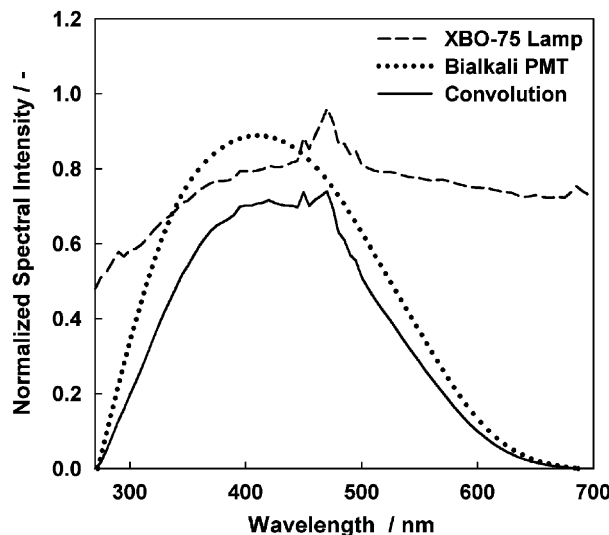


Fig. 3. Intensity spectra of the XBO-75 white light lamp and the Bi-alkali PMT used in the A10.

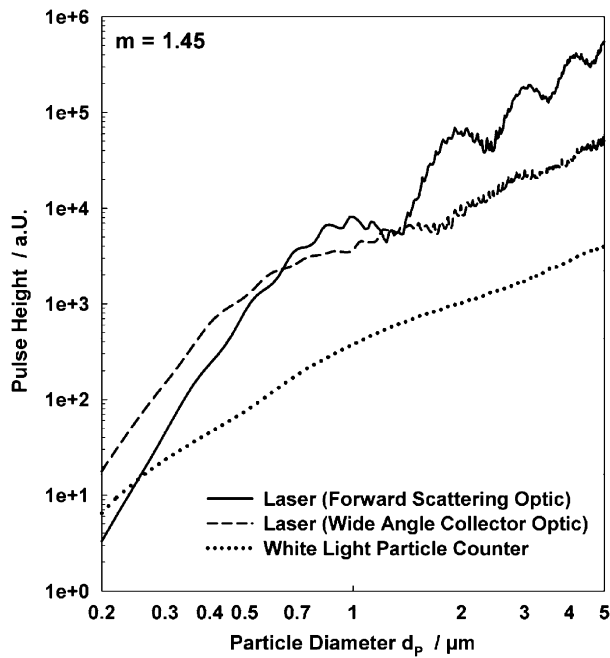


Fig. 4. Scattered light pulse height vs. droplet size ( $m = 1.45$ ) for the Grimm OPC (“wide angle”) and the A10 (“white light”; the response of the WELAS can be considered similar (in terms of smoothness) to the A10. The “forward scattering” curve is shown for comparison only. The absolute values of the pulse intensity are given in arbitrary units and therefore cannot be compared.

optics, except for the region just above 1  $\mu\text{m}$ , where some “Mie wiggles” remain. This is off-set by broadening the size classes in that region. The positive effect of the wide angle collection optic becomes evident when a comparison with the forward scattering response curve is made. However, it should be noted that the forward scattering design should, however, be less sensitive to particle, as diffracted light from the particle is principally measured (Gebhart, 1991).

### 3. Experimental methods

The calibration in terms of particle size and material was examined for each of the three OPCs by two different methods—a multimodal calibration procedure on one hand, and the common calibration using monodisperse polystyrene particles on the other. The experiments performed with PSL particles were utilised as a reference for the internal calibration of the device. By comparing the results of both methods, the influence of the refractive index can be observed, as both calibration methods are based on differing refractive indices.

In addition, the PSL-based calibration also provides a means of verifying the counting efficiencies of the three devices by comparison with a condensation particle counter (CPC; TSI Model 3010). This CPC is an absolute counting device with a nearly 100% counting efficiency above 20 nm up to several  $\mu\text{m}$  (Heim, Kasper, Reischl, & Gerhart, 2004; Wen & Kasper, 1986).

Both methods and the necessary experimental techniques are discussed more in detail below.

#### 3.1. Multimodal droplet calibration

A little-known multimodal calibration method, first presented by Chen et al. (1986), was used to simultaneously generate a test aerosol consisting of several monodisperse DEHS droplets of different sizes. To generate the test aerosol, first a relatively broad particle size distribution of DEHS (oil) was generated by atomizing (using a collision nebuliser), followed by neutralization in a bipolar Kr<sup>85</sup> charger. The droplet aerosol was then classified by means of a DMA operating at high resolution (sample:sheath flow ratio 1:10–1:40). Thereby one obtains up to eight sharp, well-defined peaks in the size spectrum, corresponding to different charge states of the particles. For one such multimodal aerosol,

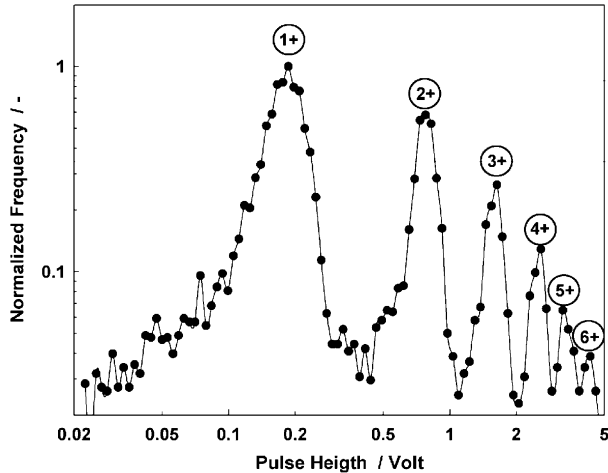


Fig. 5. Typical light scattering signal generated by the A10 for DMA classified DEHS oil aerosol. Each peak corresponds to a monodisperse size mode. The values inside the circles show the electrical charge corresponding to a peak.

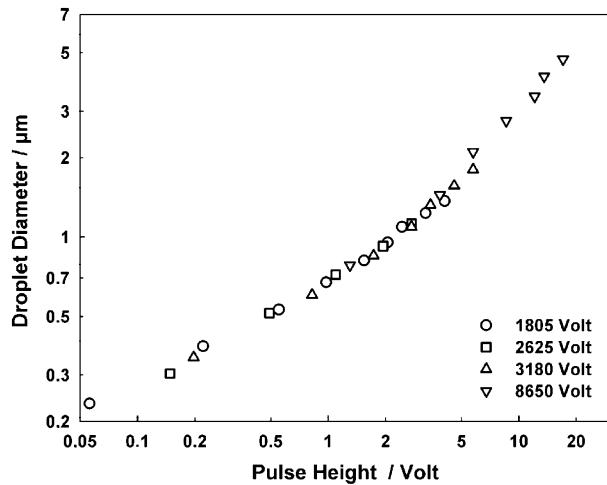


Fig. 6. Size range of DEHS droplet diameters vs. light scattering pulse height produced by each respective DMA voltage (Model A10 OPC).

**Fig. 5** shows a typical distribution of the scattered light pulse heights as measured by the A10. The principal advantage of this method is its accuracy, ease and low cost (compared to size standards) with which multiple particle classes can be obtained even well above 1  $\mu\text{m}$ , by simply altering the classifier voltage. An OPC calibration curve—such as the one shown later in **Fig. 6**—can be obtained in less than 30 min. Also, problems related to shelf-life, storage and preparation of PSL, as well as cross-contamination resulting from the use of different particle standards are avoided.

An accurate calculation of the generated particle size spectrum is possible using the following expression:

$$\frac{d_{\text{me}}}{C(d_{\text{me}})} = \frac{4 \cdot U \cdot L}{\mu \cdot \ln \left( \frac{R_1}{R_2} \right) \cdot (Q_{\text{sh}} + Q_{\text{ex}})} \cdot n \cdot e = \text{const.} \cdot U \cdot n \cdot e \quad (1)$$

where the symbols denote the electrical mobility diameter  $d_{\text{me}}$ , the applied voltage  $U$ , the dimensions of the DMA ( $R_1$ : inner electrode diameter,  $R_2$ : outer electrode diameter,  $L$ : length of the classifier), the dynamic viscosity of the gas  $\mu$  and the number of elementary charges per particle ( $n \cdot e$ ). For a given flow rate and voltage the particles in the DMA sample flow show a multimodal distribution, where the smallest peak is related to singly charged particles, the second

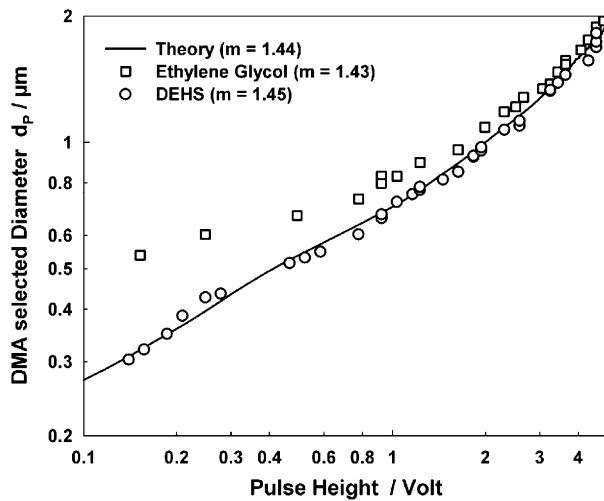


Fig. 7. DMA selected droplet diameters vs. light scattering pulse height compared with theoretical calculations.  $m = 1.44$  was used to accommodate DEHS and ethylene glycol. The evaporation of the ethylene glycol is increasingly evident towards smaller sizes.

peak for doubly charged particles and so forth. Due to the presence of the slip correction term  $C(d_{\text{me}})$ , Eq. (1) must be solved numerically to calculate the respective particle size for each charge state.

When using this method, care must be taken to prevent droplet evaporation. During a preliminary experiment, ethylene glycol was used as the calibration material, which possesses an almost  $10^6$  times higher vapour pressure than DEHS at room temperature (vapour pressure at  $20^\circ\text{C}$  for DEHS is  $1.36 \times 10^{-6}$  Pa vs.  $7.06$  Pa for ethylene glycol). Small differences in the saturation level of the sheath air used in the DMA and the subsequent dilution air were found to promote evaporation of the droplets, resulting in substantial measurement errors. This effect can be clearly observed in Fig. 7, where an increasing deviation between the theoretical pulse height and the measured signal is noticeable for ethylene glycol, but not for DEHS. As would have been expected from the Kelvin effect, the deviation increases with decreasing particles size, supporting the notion that some of the liquid evaporates between DMA and OPC. A less pronounced evaporation problem was also found when experiments were conducted using M3516 light mineral oil (Sigma Aldrich, Selze, Germany). Although the mineral oil only possesses a slightly higher (approx.  $10\times$ ) vapour pressure than DEHS, it was nevertheless found that droplets classified at 250 nm had evaporated to near 200 nm between DMA and A10 despite extensive measures to pre-saturate the air. No significant effect was found with DEHS, however, as can be observed in Fig. 7.

### 3.2. PSL-calibration and counting efficiency measurements

Each OPC was initially tested with monodisperse PSL particles using the apparatus shown in Fig. 8. Particle sizes used were 236, 305, 358, 427, 516, 783 and 972 nm, obtained from two different suppliers (postnova analytics, Landsberg/Lech, Germany and Polysciences, Inc., Warrington, USA). These sizes were verified with the DMA (operated in DMPS mode) to ensure accuracy. Agreement was usually within 5% of the sizes specified by the manufacturer; in the case of larger discrepancies the DMA determined diameter was used instead. The DMA was also utilised to remove larger agglomerates and smaller residual particles which may have been present.

For the Grimm OPC, additional measurements were performed with 1600, 1880, 2044 and 2400 nm PSL. For such large particles, it was necessary to use the DMA classification to select the doubly and triply charged particle fractions, as the voltage required for singly charged particles exceeded the capabilities of the DMA. The voltages required to select the multiply charged particles were derived from Eq. (1). For the other two OPCs, measurements with particles of this size were not possible as the yield of such large particles generated using the atomizer was extremely low, and an additional decrease in the concentration was caused by the DMA pre-classification. Due to the small measuring volumes of the A10 and the WELAS, such measurements would necessitate several hours to allow detection of a statistically significant number of particles.

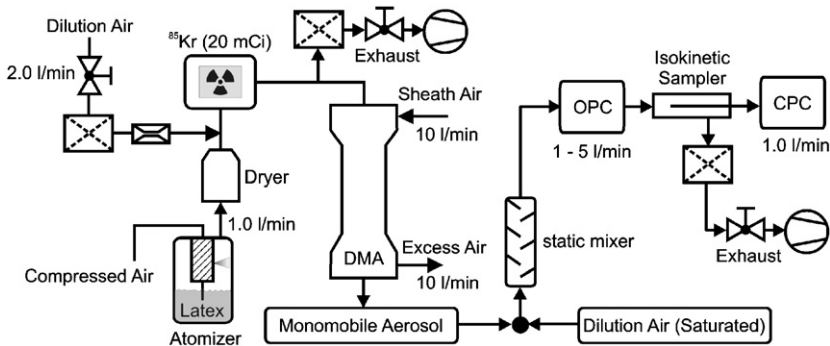


Fig. 8. Experimental set-up for calibration measurements.

Table 1  
Comparison of manufacturer specifications for OPCs examined.

OPC	Light source	Spectrum	Sample flow (l/min)	Scattering angle (range)	Spec. size range ( $\mu\text{m}$ )	Spec. max. conc. ( $\text{cm}^{-3}$ )	Counting method
A10	Osram XBO-75	White light (6000 K)	1–3	90° (64°–116°)	0.17–7.7	$1 \times 10^6$	Flux measurement
WELAS 2100	Osram Xenarc	White light (4200 K)	5	90°	0.30–40	$1 \times 10^5$	Flux measurement
Grimm 1.109	Laser diode	683 nm	1.2	90° (30°–150° and 81°–99°)	0.25–32	$2 \times 10^3$	Absolute

### 3.3. Experimental apparatus

The experimental apparatus used for both calibration procedures is shown in Fig. 8. A collision nebuliser (Topas, Dresden) was used to generate either monodisperse PSL particles or broadly polydisperse DEHS particles in various size ranges. In the case of PSL, a diffusion dryer (Topas, Dresden) was used to remove residual water vapour. Further downstream the aerosol was “neutralized” with a  $^{85}\text{Kr}$  (20 mCi) source to ensure a Boltzmann charge distribution, as it is well known that particles from atomization processes can attain relatively high charge levels (Mainelis et al., 2001). A DMA (Model Hauke “Long”, Gmunden, Austria;  $R_1 = 25\text{ mm}$ ;  $R_2 = 33\text{ mm}$ ;  $L = 600\text{ mm}$ ;  $Q_{\text{sh}} = 101/\text{min}$ ;  $Q_a = 11/\text{min}$ ), was then used to classify the aerosol according to its electrical mobility. In case of DEHS the DMA produced a multimodal test aerosol, as described above, whereas in the case of PSL particles, the DMA was used merely to remove agglomerated particles (doublets, triplets) as well as small residual particles from the atomization process.

Depending on the flow rate required (which in turn depended on the instrument to be examined), the monomobile particles (particles of one given electrical mobility) exiting the DMA were diluted by a stream of particle free air and subsequently mixed in a static mixer. The additional mixing helped to avoid concentration fluctuations caused by laminar layering. When DEHS droplets were used as the calibration material, the dilution air was pre-saturated with DEHS by passing it through a fibrous filter medium connected to a bath of DEHS, to avoid droplet evaporation by the mixing with unsaturated air. For the same reason, sheath air and excess air of the DMA were run in a closed loop configuration with a similar saturator when DEHS droplets were being used.

As seen from Table 1, the three devices are designed to operate at different flow rates. This necessitated two different calibration set ups, according to the flow rate required. The A10 and the WELAS were placed in the “OPC” position as shown in Fig. 8, followed by an isokinetic sampler connected to a TSI 3010 CPC. For the examination of the Grimm OPC another configuration was used (not shown), where the A10 was placed after the static mixer followed by a flow divider which fed 1.2 l/min to the Grimm device and another 1.0 l/min to the TSI CPC. This was necessary because the internal filter of the Grimm OPC prevents it from being used in line. The flexibility of the A10 (with respect to

operational flow rate) allowed it to be calibrated at two different flow rates—revealing no difference in the results gained by either method (with the exception of counting efficiency—discussed later).

#### 4. Results and discussion

##### 4.1. Pulse height calibration using PSL and DEHS

The WELAS and A10 OPCs were tested using seven sizes of PSL between 236 and 972 nm (however, the WELAS was unable to detect the smallest size at 236 nm); the Grimm OPC was additionally tested with four larger sizes as mentioned previously.

**Fig. 9** shows the measured PSL particle sizes compared to the internal calibration. Both white light devices—the A10 and the WELAS—size these particles with a high degree of accuracy in the measured range of up to about 1 μm. For the laser device Grimm 1.109, the sizing accuracy decreases from around 0.8 μm up to approximately 2 μm, probably due to the occurrence of the said undulations in the calibration curve. Broader size channels/classes than are likely currently implemented for the particular size range may reduce this problem for the sizing of PSL particles. For the smallest observed datum, it is believed that the measured signal is influenced by counting efficiency and coincidence effects. Single particles of the smallest size (236 nm) are most likely not counted, as their scattering intensity is below the electronic trigger threshold. However, coincident particles that enter the measuring volume simultaneously produce a higher signal (through signal addition) which would be above the trigger threshold.

An analysis of the measured pulse heights as a function of PSL diameter can give more insight regarding the cause of these deviations for the Model 1.109 OPC. (Pulse heights for each of the 32 channels were supplied by the manufacturer on request and are gratefully acknowledged.) The direct comparison between the theoretical response function discussed in the preceding section and the measured pulse heights for PSL particles is shown in **Fig. 10**, together with the corresponding curves for the A10 and the WELAS. (A manufacturer supplied calibration curve was used for the WELAS, since the data necessary to calculate the response by Mie theory was unavailable.) Evidently, for all three instruments the measured pulse heights for PSL particles lie on or very close to the calculated response curves. In particular, for the Grimm 1.109, the response curve shows the expected flattening in the range of about 0.7–2.0 μm, which leads to the aforementioned differences. Broader size channels/classes (than are currently implemented for that particular size range) would reduce this behaviour, at least for particles with a refractive index comparable to PSL particles. (Altering the refractive index may alter the slope or position of this section of the curve.)

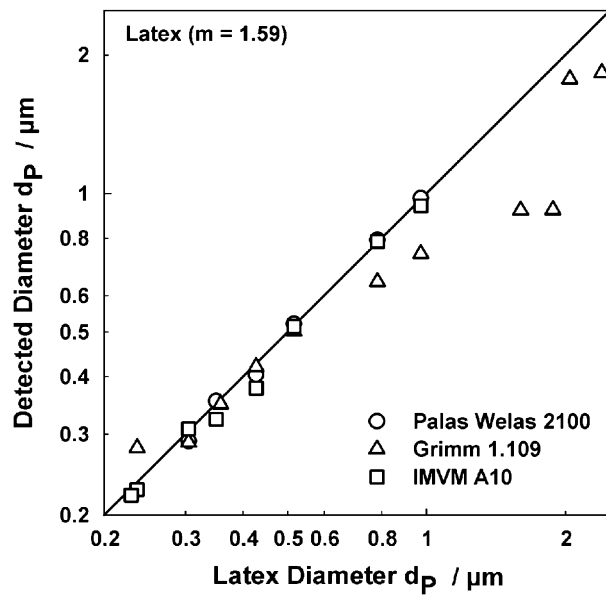


Fig. 9. Detected vs. actual PSL diameter for the three OPCs tested. The detected size is based on the internal calibration of each device.

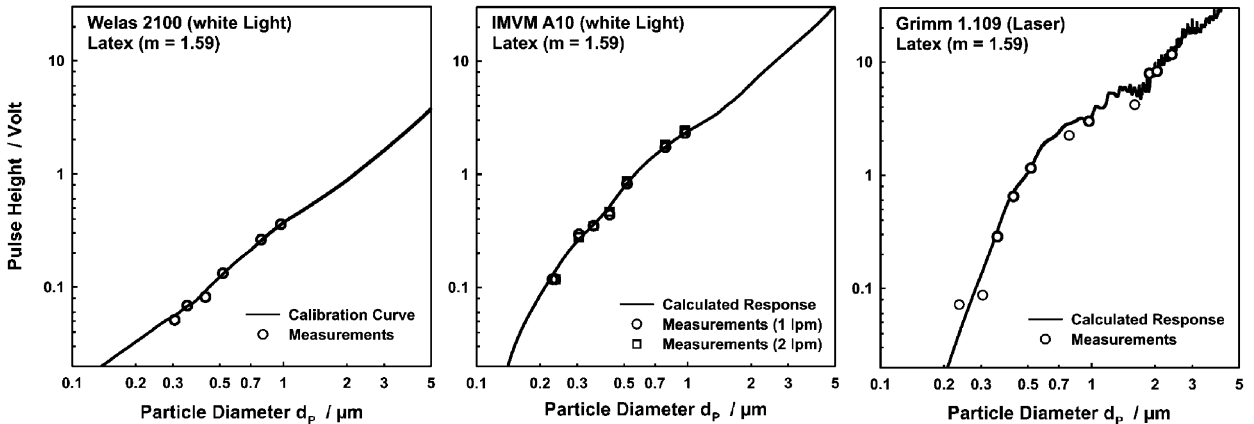


Fig. 10. Comparison of measured scattered light pulse heights with calculated response curves based on Mie theory for PSL particles ( $m = 1.59$ ).

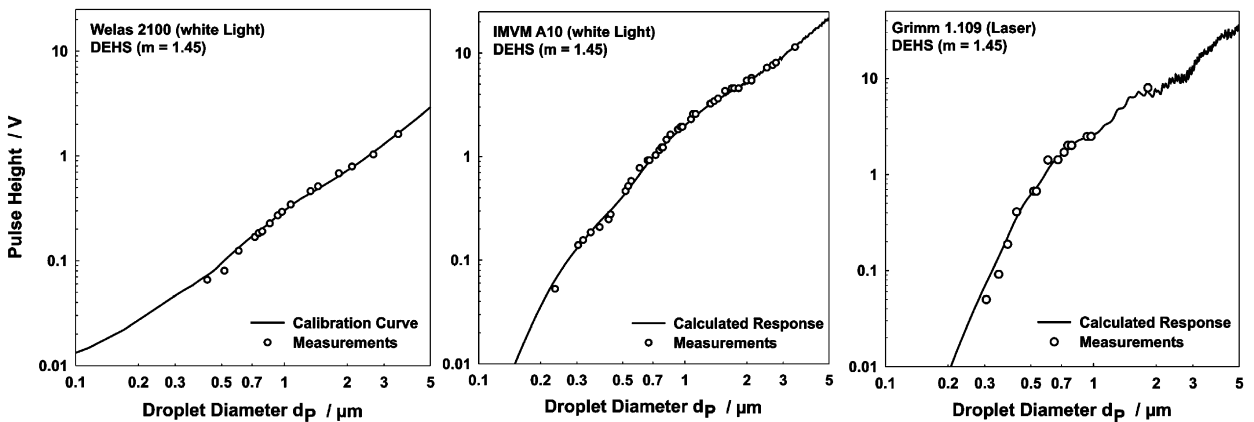


Fig. 11. Comparison of measured scattered light pulse heights with calculated response curves based on Mie theory for DEHS droplets ( $m = 1.45$ ).

The comparison data for DEHS aerosol using the multimodal droplet method are shown in Fig. 11. Care was taken to select roughly the same droplet size range as before for the measurements with PSL, and to use the identical droplet sizes for all three devices. Again all pulse heights lie on or very close to the calculated response curve, now calculated for the refractive index of DEHS. Note that the number of data points varies between curves, due to the differing device sensitivities in detecting the larger droplets. Due to the lower channel resolution (31 channels), the Model 1.109 OPC was not able to resolve more than a maximum of three peaks, hence 14 data points being present on the Grimm curve. The WELAS (16 data points) showed a higher resolving power, and was consistently able to detect at least up to triply-charged particles, whereas the A10 was in some instances able to detect up to sixfold or eightfold charged particles (refer Fig. 5 for typical A10 data).

#### 4.2. Counting efficiency measurements With PSL particles

Counting efficiencies are shown in Fig. 12. The Model 1.109 OPC has a counting efficiency which decreases from 100% above 780 nm to approximately 90% at 305 nm, and then drops off steeply below 305 nm. The particle concentration used for the above measurements was  $< 400 \text{ p}/\text{cm}^3$  for the Grimm and  $< 1000 \text{ p}/\text{cm}^3$  for the other two devices, so as to ensure that coincidence effects did not influence the results. As PSL particle suspensions have increasing number concentrations with decreasing particle size, the coincidence effect became more pronounced for the smaller sizes. When this was detected, the concentration for the 305 nm particles was reduced in steps until the counting efficiency became stable.

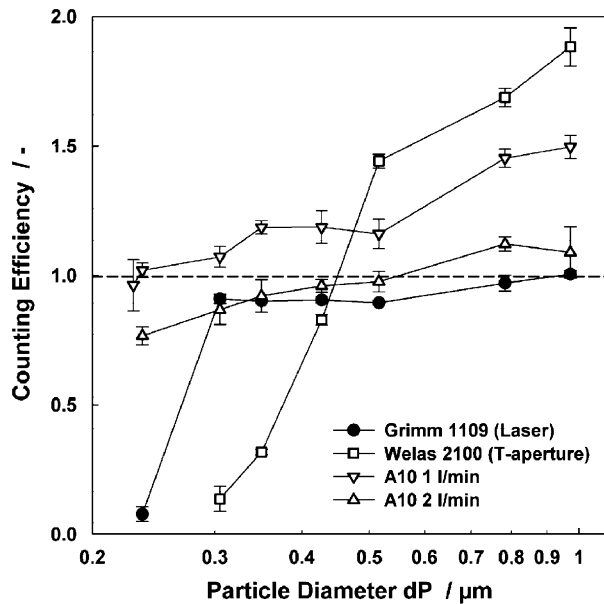


Fig. 12. Counting efficiency vs. particle size, based on measurements with PSL particles. (For the A10 two different flow rates are shown.) Each data point represents an average of 3–5 repetitions.

The two white-light OPCs both exhibit upward sloping efficiency curves; towards larger particle sizes a significant part of the curve lies well above 100%. In both cases, this effect is due to their design. An optically defined sensing volume (a cube for the A10; a T-shaped volume for the WELAS; compare Fig. 1) is generated by crossing an appropriately shaped beam of light at right angle with a shaped “beam of observation”. The shaping is done with diaphragms and although the resulting edge definition is quite sharp, a finite transition zone of a few micrometers remains nevertheless between illuminated and non-illuminated zones, which may in effect become enlarged due to misalignment problems. Hence large particles are more likely to remain be detectable when passing just outside the theoretical measurement volume than very small particles. (Although the large particles would appear optically smaller, due to the sharply decreasing intensity of illumination outside the sensing volume.) In any case, such an effect (even if small as in the case of the A10) would tend to be more pronounced as particle size increases; hence the upward sloping curves. (In principle, one could also envisage another, secondary effect resulting from focussing of the flow field. This is less likely, however, and will not be pursued further in the context of this paper.) Such elevated counting efficiency results from non-absolute-counting OPCs have been reported previously (Gebhart, Blankenberg, Bormann, & Roth, 1983; Sachweh et al., 1998).

According to Fig. 12, the WELAS OPC shows a much steeper change in counting efficiency than the A10. This is likely due to differences in design such as a lower intensity and different wavelength of the illumination light source, as well as additional loss of light intensity provided by the optic fibres. The A10, by comparison shows a relatively flat counting efficiency relationship. Furthermore, for a flow rate of 2 l/min, the counting efficiency of the A10 does not increase significantly above 100%, suggesting that the twin photomultiplier method is more successful than the T-shaped measuring volume in permitting erroneous particles to be excluded from data—in terms of the measured particle concentration. For the lower flow rate, however, the A10 also exhibited pronounced over-counting of particles. One explanation for this observation is based on the electronic circuit used within the A10, which demands a defined minimum signal length above the electronic trigger level to count a valid particle. Particles passing through the less illuminated outer parts of the border zone are unlikely to produce a signal length long enough to be counted as a valid particle and are therefore discarded. As this criteria is directly related to the residence time of the particle in the border zone and hence with the flow rate, the observed increase in counting efficiency for the lower flow rate could be due to this effect. Further investigation is necessary, to determine which of these factors is the cause of this effect in the A10. In terms of sizing errors caused by the border zone, the T-shaped measuring volume clearly performs better (not shown), as already demonstrated by Mölter and Keßler (2004a).

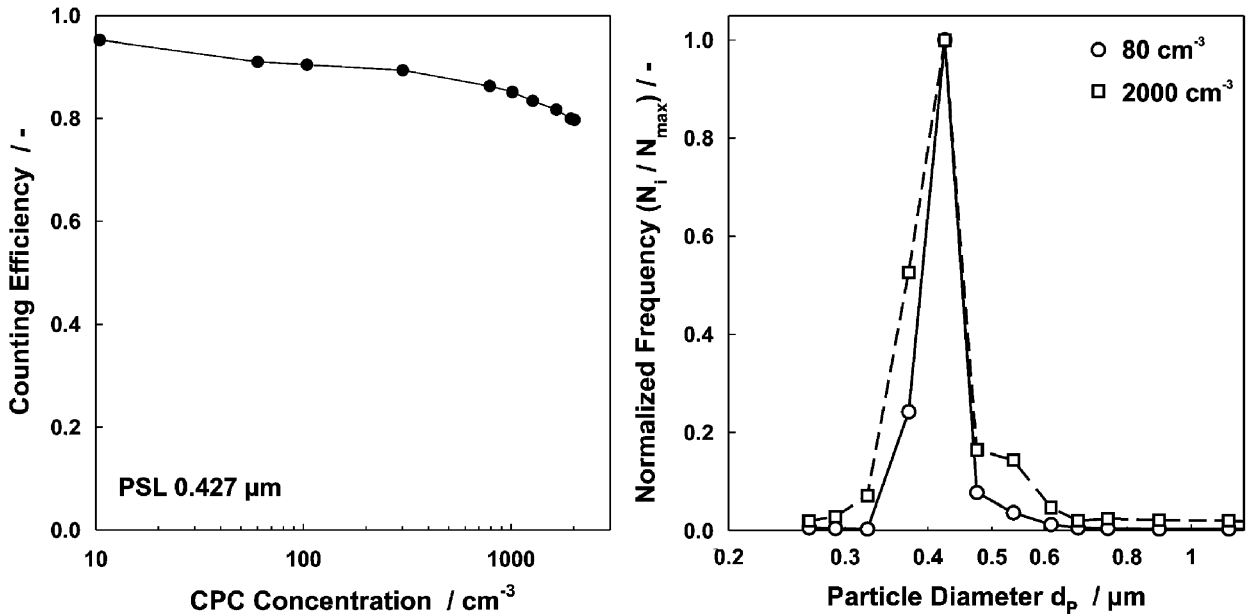


Fig. 13. Loss in counting efficiency due to coincidence error for the Model 1.109 OPC (left), and apparent broadening of the measured size distribution with increasing concentration (for 427 nm PSL particles).

The curves shown in Fig. 12 can be used to incorporate a counting efficiency correction into the data processing software of an OPC. Neither of the commercial counters available for evaluation had such a correction built in.

#### 4.3. Coincidence effects (1.109 OPC only)

Coincidence effects were noticed with the 1.109 OPC during the counting efficiency measurements. This effect was quantified using 427 nm PSL particles. Fig. 13 shows the coincidence error for the Grimm 1.109 device—measurements with the other OPCs were not possible, as PSL could not be nebulised in sufficiently high concentration, and the reference instrument (TSI Model 3010 CPC) will itself encounter coincidence-induced counting efficiency problems when operated at  $1 \times 10^4 \text{ p/cm}^3$  or higher (Heim et al., 2004). The approximate reduction in counting efficiency due to coincidence reached a level of 20% at  $2 \times 10^3 \text{ p/cm}^3$ . This is also the upper concentration limit specified by the manufacturer. This corresponded with broadening of the particle size distribution (see Fig. 13)—a typical effect of coincidence (Raasch & Umhauer, 1984).

## 5. Conclusions

A little-known method for efficient size calibration of OPCs, first mentioned by Chen et al. (1986), was shown to be far superior to the classical PSL calibration—especially for instruments with a high resolving power. The method effectively permits the simultaneous generation of up to eight precisely known particle diameters including sizes well above 1  $\mu\text{m}$ .

The method was used with DEHS oil aerosol (in conjunction with PSL spheres), in order to examine the performance of three widely used OPCs. The results show that all devices were able to size the PSL aerosol accurately (Fig. 10). A calibration curve for the widely used DEHS oil was also obtained.

In terms of the accuracy and sensitivity in detecting and sizing the DEHS aerosol, the UKA A10 clearly performed best, the WELAS Model 2100 second, and the Grimm Model 1.009 OPC third. (Being a laser device, the latter is disadvantaged slightly by undulations in the optical response curve known to result in the Mie scattering region. This was shown by comparing measured pulse heights with theoretically calculated response curves, where possible.)

Counting efficiencies of the three devices were also obtained (Fig. 12). Only the Grimm Model 1.109 had an efficiency within 10% of the ideal 100%. The two other counters showed systematic deviations (in case of the Model 2100 very substantial deviations) requiring a software correction during data processing, similar to the SMPS. Unlike the WELAS, the Grimm OPC currently does not permit the incorporation of user-defined calibrations for refractive index or counting efficiency.

## Acknowledgments

The authors would like to thank Dominik Nagel from the Universität Karlsruhe, Institut für Technische Thermodynamik und Kältetechnik for the loan of the Palas WELAS 2100 and assisting with its testing. The authors would also like to thank the laboratory and technical staff from the Institut für Mechanische Verfahrenstechnik und Mechanik, in particular, Luana Deambrosi, Friedhelm Klingel and Karl-Heinz Weiss for their valuable assistance.

## References

- Bohren, C. F., & Huffman, D. R. (1998). *Absorption and scattering of light by small particles*. Berlin: Wiley-VCH.
- Card, J. B. A., & Jones, A. R. (1991). Measurement of the refractive-index of atomized liquid-drops by light-scattering. *Particle & Particle Systems Characterization*, 8(4), 267–273.
- Chen, B. T., Cheng, Y. S., & Yeh, H. C. (1986). Experimental responses of 2 optical-particle counters. *Journal of Aerosol Science*, 15(4), 457–464.
- Dittler, A. (2001). Gasreinigung mit starren Oberflächenfiltern-Erscheinungsformen und Auswirkungen unvollständiger Filterregenerierung. *Chemical and Process Engineering*. Karlsruhe, Universität Karlsruhe. Doctor of Engineering.
- Gebhart, J. (1991). Response of single-particle optical counters to particles of irregular shape. *Particle & Particle Systems Characterization*, 8(1), 40–47.
- Gebhart, J., Blankenberg, P., Bormann, S., & Roth, C. (1983). Vergleichsmessungen an optischen Partikelzählern. *Staub, Reinhalterung der Luft*, 43, 439–448.
- Heim, M., Kasper, G., Reischl, G. P., & Gerhart, C. (2004). Performance of a new commercial electrical mobility spectrometer. *Aerosol Science and Technology*, 32(S2), 3–14.
- Mainelis, G., Willeke, K., Baron, P., Reponen, T., Grinshpun, S. A., Gorny, R. L. et al. (2001). Electrical charges on airborne microorganisms. *Journal of Aerosol Science*, 32(9), 1087–1110.
- Mölter, L., & Munzinger, F. (1998). European Patent EP0823626. Device and method for measuring particle fluxes in a fluid. Patentowner: Palas GmbH.
- Mölter, L., & Keßler, P. (2004a). Determination of the particle size and particle number in the outside air by means of a new optical aerosol spectrometer. *Gefahrstoffe Reinhalterung Der Luft*, 64(10), 439–447.
- Mölter, L., & Keßler, P. (2004b). Basics of the particle size and particle number determination in outside air with counting measuring methods. *Gefahrstoffe Reinhalterung Der Luft*, 64(7/8), 319–323.
- Nagy, A., Szymanski, W. W., Gal, P., Golczewski, A., & Czitrovszky, A. (2007). Numerical and experimental study of the performance of the dual wavelength optical particle spectrometer (DWOPS). *Journal of Aerosol Science*, 38(4), 467–478.
- Raasch, J., & Umhauer, H. (1977). Fundamental considerations in measurement of particle-size and particle velocity of dispersed phases in flow systems. *Chemie Ingenieur Technik*, 49(12), 931–941.
- Raasch, J., & Umhauer, H. (1984). Der Koinzidenzfehler bei der Streulicht-Partikelgrößen-Zählanalyse. *VDI-Fortschrittsberichte*. Reihe 3, Nr. 95.
- Sachweh, B., Umhauer, H., Ebert, F., Buttner, H., & Friemelt, R. (1998). In situ optical particle counter with improved coincidence error correction for number concentrations up to 10<sup>7</sup> particles cm<sup>-3</sup>. *Journal of Aerosol Science*, 29(9), 1075–1086.
- Umhauer, H., Berbner, S., & Hemmer, G. (2000). Optical in situ size and concentration measurement of particles dispersed in gases at temperatures up to 1000 degrees C. *Particle & Particle Systems Characterization*, 17(1), 3–15.
- Umhauer, H., Meyer, J., & Schiel, A. (2008). A novel device for single particle scattering size analysis and concentration measurement at high pressures and temperatures. *Particle Systems Characterisation*, 25(2), 119–135.
- Vetter, T. (2004). *Berechnung der Mie-Streufunktionen zur Kalibrierung optischer Partikelzählgeräte*. Diploma thesis, Johannes Gutenberg-Universität, Mainz.
- Wen, H. Y., & Kasper, G. (1986). Counting efficiencies of 6 commercial particle counters. *Journal of Aerosol Science*, 17(6), 947–961.